TISSUE ENGINEERING
Volume 12, Number 11, 2006

Magnetically-Guided Self-Assembly of Fibrin Matrices with Ordered Nano-Scale Structure for Tissue Engineering

EBEN ALSBERG, Ph.D.,[1*] EFRAIM FEINSTEIN, B.Sc.,[2] M. P. JOY, Ph.D.,[1] MARA PRENTISS, Ph.D.,[2] and DONALD E. INGBER, M.D., Ph.D.[1]

ABSTRACT

The development of effective biological scaffold materials for tissue engineering and regenerative medicine applications hinges on the ability to present precise environmental cues to specific cell populations to guide their position and function. Natural extracellular matrices have an ordered nano-scale structure that can modulate cell behaviors critical for developmental control, including directional cell motility. Here we describe a method for fabricating fibrin gels with defined architecture on the nanometer scale in which magnetic forces are used to position thrombin-coated magnetic micro-beads in a defined 2-dimensional array and thereby guide the self-assembly of fibrin fibrils through catalytic cleavage of soluble fibrinogen substrate. Time-lapse and confocal microscopy confirmed that fibrin fibrils nucleate near the surface of the thrombin-coated beads and extend out in a radial direction to form these gels. When controlled magnetic fields were used to position the beads in hexagonal arrays, the fibrin nano-fibrils that polymerized from the beads oriented preferentially along the bead—bead axes in a geodesic (minimal path) pattern. These biocompatible scaffolds supported adhesion and spreading of human microvascular endothelial cells, which exhibited co-alignment of internal actin stress fibers with underlying fibrin nano-fibrils within some membrane extensions at the cell periphery. This magnetically-guided, biologically-inspired microfabrication system is unique in that large scaffolds may be formed with little starting material, and thus it may be useful for *in vivo* tissue engineering applications in the future.

INTRODUCTION

ORDERED ARRANGEMENTS OF EXTRACELLULAR MATRIX (ECM) are found in all solid tissues *in vivo*, including bone,[1] cartilage,[2] dental enamel,[3] and the basement membranes that line epithelial and endothelial tissues.[4] Ordered ECM structures are important for guiding cellular behavior *in vivo*, such as orienting cell motility during neurogenesis,[5] epitheliogenesis,[6] and angiogenesis.[7] These findings have been attributed to a mechanism termed "contact guidance,"[8] in which anisotropic material properties can elicit a directional cellular response.[9] The nano-meter scale structure of materials also determines their mechanical behavior.[10] The ability to develop biocompatible materials or artificial ECMs with defined nano-structure may therefore have significant value for tissue engineering and regenerative medicine.

Although these ordered structures are commonplace in living materials, reproducing them in the laboratory remains difficult.[11] Several methods have been used to orient fibrous proteins to replicate the nano-scale architecture of organized ECM networks observed *in vivo*. These methods include template-directed assembly,[12] cell-induced compaction,[13] the application of external cyclical mechanical forces,[14] reverse dialysis[15] or evaporation[16] (to promote liquid crystalline assembly), and the application of strong magnetic

[1]Vascular Biology Program, Children's Hospital/Harvard Medical School, Boston, Massachusetts.
[2]Department of Physics, Harvard University, Cambridge, Massachusetts.
*Current address: Department of Biomedical Engineering, Case Western Reserve University, Cleveland, Ohio.

fields to orient protein fibers with diamagnetic anisotropy.[9,17] Some of these oriented biopolymer networks have been shown to produce oriented fibrillar ECM materials that control cell orientation,[18] extension,[9,19] and migration[20] *in vitro* through contact guidance. However, a single axis of alignment usually dominates the microstructure of these materials, and control over the 3-dimensional (3D) organization of a supramolecular ECM lattice on the nano-meter scale has not been reported.

Various biomolecules, including peptides, lipids, and enzymes, have been used to self-assemble gel networks for tissue engineering and drug-delivery applications.[21–26] In the present study, we developed a method to spatially control the self-assembly of fibrin lattices. Fibrin plays a critical role in tissue development, hemostasis, angiogenesis, and wound repair. Fibrin clots (3D matrices composed of fibrin) are formed when thrombin—a downstream enzyme in the coagulation cascade—cleaves the plasma glycoprotein fibrinogen to release fibrin protein. Continuous thrombin activity increases the concentration of soluble fibrin monomers and induces them to self-assemble into linear polymers called protofibrils. Protofibrils subsequently aggregate laterally and become covalently bonded to form fibrin fibers and lattices that make up the backbone of the fibrin clot.[27] Fibrin clots form physiologically at sites of blood vessel damage, where they immediately prevent bleeding and later promote angiogenesis and tissue repair.[28] They also form at sites of bone fracture, where they facilitate regeneration in the fracture callus, and nerve cells can use fibrin clots as an ECM bridge to repair severed nerves.

Because fibrin plays a critical role in many natural healing processes, it has been investigated extensively as a biological scaffold for bone,[29,30] cartilage,[31] neural,[32] adipose,[33] and blood vessel[34,35] regeneration. These studies have revealed that the structure and morphology of fibrin networks (i.e., fiber size, branching, fiber spacing) influence their physical properties (e.g., viscoelasticity[36]) and biological functionality,[37] including their ability to support nerve growth,[38] leukocyte migration,[39] and capillary morphogenesis[40–42] *in vitro*. Here, we describe a method to spatially constrain the fibrin self-assembly process on the nanometer-to-micro-meter scale by using magnetic fields to orient thrombin-coated magnetic micro-beads. Although enzymes are often coupled to magnetic beads for biochemical applications,[43] they have not been used to catalyze the formation of ECMs with oriented microstructure. In this study, an external magnetic field was used to organize superparamagnetic micro-beads coated with thrombin into a 2-dimensional (2D) periodically ordered geodesic array at the air—liquid interface of a fibrinogen solution. The external magnetic field controlled the lattice shape and spacing. Over a period of minutes, enzymatic cleavage of fibrinogen by the bead-immobilized thrombin enzyme caused the released fibrin molecules to self-assemble into a 3D fibrin lattice with nanometer-scale fibrin fibrils oriented in a fully repeating triangular pattern that closely mimicked the arrangement of the beads. This method may prove useful for rapid fabrication of large-scale (mm to cm) fibrin-based biomaterials with defined micro- and nano-structure for tissue engineering applications.

MATERIALS AND METHODS

Micro-Bead Preparation

Tosyl-activated superparamagnetic beads (4×10^7 beads/100 μL; 4.5 μm diameter; Dynal Biotech, Oslo, Norway) were washed with phosphate buffered saline (PBS) without calcium or magnesium (Invitrogen Corporation, Carlsbad, CA), reconstituted in carbonate buffer (pH 9.4), and combined with 300 μL of bovine plasma thrombin (50 U/mL; Sigma, St. Louis, MO) containing 0.1% bovine serum albumin (BSA; Intergen, Purchase, NY). After incubation for 24 h at 4°C, the beads were washed with 0.1% BSA in PBS and resuspended in 100 μL of the BSA solution. Control beads were prepared by leaving thrombin out of the 0.1% BSA solution.

Measurement of thrombin-coating efficiency

H-D-Phenylalanyl-L-pipecolyl-L-arginine-p-nitroaniline dihydrochlorine (H-D-Phe-Pip-Arg-pNA 2HCl; Diapharma Group, Inc., West Chester, OH) was used as a thrombin-specific chromogenic substrate to measure thrombin activity. In this assay, 50 μL of standard or experimental solution and 50 μL of chromogen buffer containing 50 mM tris(hydroxymethyl)-aminomethane (Bio-Rad Laboratories, Hercules, CA) and 150 mM sodium chloride (Sigma) at pH 8.3 were mixed with 50 μL of chromogenic substrate (2 mM), incubated at 37°C for 2 min, and quenched with 50 μL of 20% (vol/vol) glacial acetic acid (Sigma). Sample optical absorbance was measured at 405 nm on a SpectraMax 190 spectrophotometer (Molecular Devices, Sunnyvale, CA). Thrombin activity was measured at least in duplicate in 3 separate bead preparations and in samples from 6 wash steps in 2 independent bead preparations. Beads were magnetically removed from samples before quantification.

Dependence of clot size on bead number

Fibrinogen from bovine plasma (Sigma) was reconstituted at 10 mg/mL in 0.9% (w/vol) sodium chloride (NaCl), sterilized by filtration through a Nalgene (0.22 μm) filter, and dispensed into aliquots for storage at −20°C. In all experiments involving fluorescence microscopy, fibrinogen conjugated to Alexa Fluor-488 (10 mg/mL; Molecular Probes, Eugene, OR) was mixed 1:1000 with the unconjugated fibrinogen solution before use. Small aliquot (2 μL) solutions containing different numbers (1.6, 3.8, 13.4, or 80.0×10^4) of thrombin-coated beads were placed on the bottom of a 35-mm tissue-culture dish (Becton

Dickinson, Franklin Lakes, NJ), and 200 μL of fibrinogen solution was dispensed on top of the beads. Samples were incubated for 100 min at 37°C with 5% carbon dioxide (CO_2), fixed in 4% paraformaldehyde solution (Electron Microscopy Sciences, Hatfield, PA), stained for 10 min with Coomassie Brilliant Blue (0.031%; Bio-Rad) in 50% methanol (Fisher Scientific, Pittsburgh, PA) and 8.75% glacial acetic acid, and photographed with a D-490 digital camera (Olympus, Tokyo, Japan) or an Eclipse E600 upright microscope (Nikon, Tokyo, Japan) equipped with a Spot Insight Color Digital Camera (Diagnostic Instruments, Inc., Sterling Heights, MI). Photomicrographs of fibrin fibril nucleation from the surface of the beads were obtained with a small number (3.8×10^4) of beads using differential interference contrast (Nomarski) imaging every 30 sec for 40 min with an Eclipse 2000-E inverted microscope (Nikon) equipped with a Photometrics CoolSnap HQ digital camera (Roper Scientific, Inc., Duluth, GA) and IPLab image-acquisition and processing software (BD Biosciences, Rockville, MD). Additional images were obtained on a DM IRE2 confocal microscope with a TCS SP2 acousto-optical beam splitter (Leica, Northvale, NJ).

Quantification of bead order

To measure magnetic field—induced bead reorientation, 136 μL of fibrinogen solution (10 mg/mL) was combined with 4 μL of 0.1% Triton-X-100 (Sigma), 8 μL of 150 mM calcium chloride (CaCl, Sigma), and 2 μL of thrombin-coated beads (1.9×10^7 beads/mL); the solution was then placed in a single-chamber Lab-Tek glass slide with cover (Nagle Nunc International, Rochester, NY) and incubated at 37°C for 2 h in the presence or absence of the stationary magnetic array system at a 2-cm distance (Fig. 1). The magnetic array system was composed of a neodymium-iron-boron nickel-coated ring magnet (0.750" outer diameter (OD)×0.410" inner diameter (ID)×0.375" thick, 0.5 T peak field at the magnet surface, Master Magnetics, Castle Rock, CO) placed on top of an iron washer (0.750" OD×0.125" ID×0.125" thick). Resultant fibrin clots were fixed, and images were recorded on the Eclipse 2000-E microscope. The fibrinogen and CaCl solutions were in a 150-Mm NaCl, 10 mM N-2-hydroxyethylpiperazine-N′-2-ethanesulfonic acid (Sigma) buffer (pH 7.4) for this part of the study only. Ideal magnetic field–induced bead arrays used as controls were formed with uncoated beads in PBS solution (i.e., rather than fibrinogen solution) maintained at 23°C for 1 h. A thresholding IPLab script was used to identify the coordinates of the bead centers in photomicrographs from 3 different regions of 3 separate samples, and a program written in MatLab computer software (The MathWorks, Inc., Natick, MA) determined the distance between each bead and its 3 nearest neighbors.

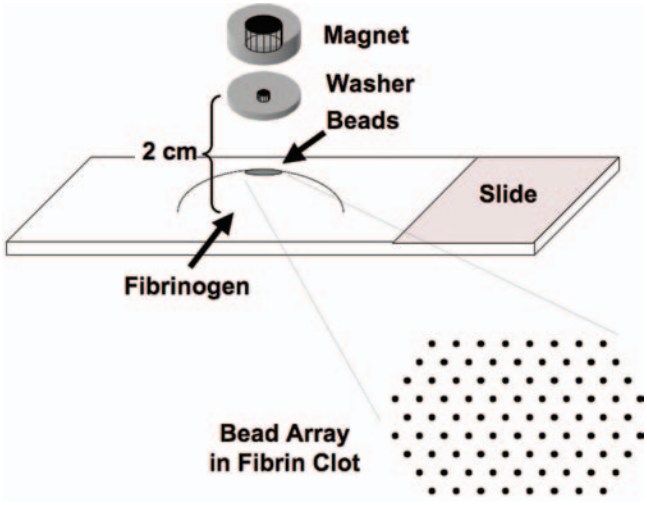

FIG. 1. Schematic diagram of the magnetic bead array guidance system. Color images available online at www.liebertpub.com/ten.

Quantification of fibrin fibril orientation

To analyze the nano-structure of the fibrin gels, 143 μL of fibrinogen solution (10 mg/mL) was combined with 5 μL of 0.1% Triton-X-100 and 2 μL of thrombin-coated beads (1.9×10^7 beads/mL). The solution was placed on a Lab-Tek glass slide and incubated at 37°C for 7 to 14 h approximately 2 cm below the bottom of the magnet. The resultant fibrin array clots were then incubated in endothelial basal medium-2 (EBM-2; Cambrex Bio Science Walkerville, Inc., Walkerville, MD) for 5 to 20 h at 37°C with 5% CO_2, fixed, and mounted under CoverWell imaging chamber gaskets (Molecular Probes) with Fluoromount-G (Southern Biotechnology Associates, Inc., Birmingham, AL).

To determine whether fibrin fibrils preferentially oriented along the main bead–bead axes, Z-stacks of confocal images identifying triangular bead arrangements were flattened into a composite projection image to capture the fibrin clot 3D architectural features. A grid of squares was overlaid on these images with its long axis parallel to a line drawn between the beads constituting the triangle or with the long axis parallel to a line drawn between 1 bead and the midpoint of the opposite side linking the 2 remaining beads of the triangle. Fibrin fibril intersections with the vertical (V) and horizontal (H) grid lines, and values for the total lengths of these lines (TV and TH, respectively), were used to calculate an orientation ratio (V/TV:H/TH). Orientation ratios were obtained from 4 different locations in 2 separate bead arrays.

Cell culture on nano-structured clots

Human microvascular endothelial cells from neonatal dermis (passage ≤8, Cascade Biologics, Inc., Portland, OR) were cultured in endothelial basal medium-2 supplemented with microvascular endothelial cell growth medium (EGM-2 MV). Cultures were maintained at 37°C in a humidified atmosphere with 5% CO_2. Cells were seeded

onto fibrin clot bead arrays (6,000–25,000 cells/mL) created using the magnetic fabrication technique; after 2 days, clots were washed with EGM-2 MV, fixed with 4% paraformaldehyde, and permeabilized with 0.2% Triton-X and 0.1% BSA in PBS before staining of actin with Alexa Fluor-594 phalloidin and nuclear staining with 4′,6-diamidino-2-phenylindole (1 μg/mL in PBS, Molecular Probes).

Statistics

All results are reported as means ± standard errors of the mean; statistical analysis was performed using the 2-tailed Alternate Welch *t*-test, with statistical significance defined as $p < 0.01$.

RESULTS

Bead-immobilized thrombin is active

Magnetic micro-beads (4.5 μm diameter) that were coated with thrombin (7.4×10^{-9} units/bead) via tosyl cross-linking were found to retain high levels of thrombin activity when analyzed using an amidolytic assay to measure the level of cleavage of the synthetic tripeptide substrate S-2238 (Fig. 2). In contrast, control beads that lacked thrombin had virtually no activity, and analysis of bead washes confirmed that thrombin-coated beads that were washed more than 4 times failed to release any significant soluble thrombin activity (Fig. 2).

Incubation of the thrombin-coated magnetic micro-beads with soluble fibrinogen resulted in formation of fibrin clots containing multiple isolated beads, or small groups of beads, separated by large areas filled with a dense lattice of fibrillar proteins, as detected by staining with Coomassie Brilliant Blue (Fig. 3A). The size of the clot also increased as the bead number was raised from 1.6 to 80.0×10^4 beads in the 200 μL of fibrinogen solution, resulting in macroscopic clots approximately 1 mm to 1 cm in diameter (Fig. 3B-E). In contrast, addition of an equal volume of bead supernatant from the solution of washed thrombin-coated beads failed to form any detectable clot (not shown). Similar results were also obtained by covalently coupling thrombin to nanometer-sized (100 or 250 nm diameter) carboxylated beads (Kisker-Biotech, Steinfurt, Germany) using carbodiimide chemistry (not shown).

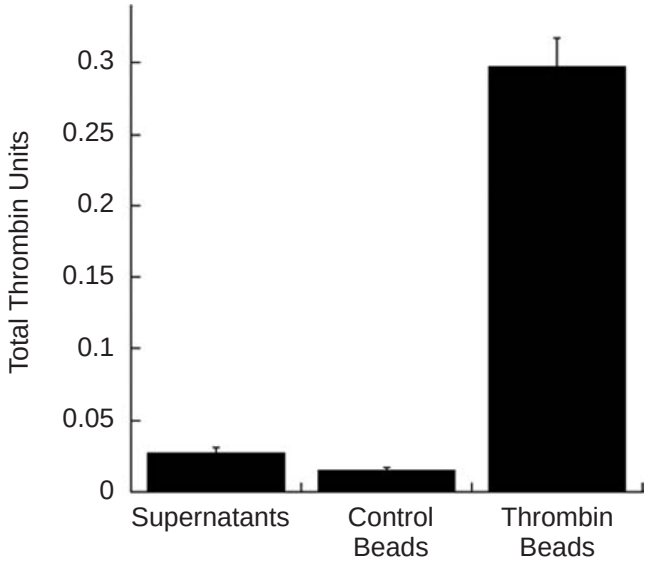

FIG. 2. Graph showing thrombin enzymatic activity: 4.5 μm diameter magnetic micro-beads covalently linked to thrombin (thrombin beads) compared with supernatant washes (supernatants) and uncoated samples (control beads).

Origin of clot nucleation

Nomarski microscopy was carried out to analyze the spatial pattern of clot formation. Time-lapse recording revealed that the first fibrils appeared near the surface of each bead within 10 min after fibrinogen addition and that these fibrils continued to grow and extend until they eventually coalesced with fibrils extending from the surface of neighboring beads to form a dense fibrillar lattice (Fig. 4A-D). A representative confocal image of a clot formed in this

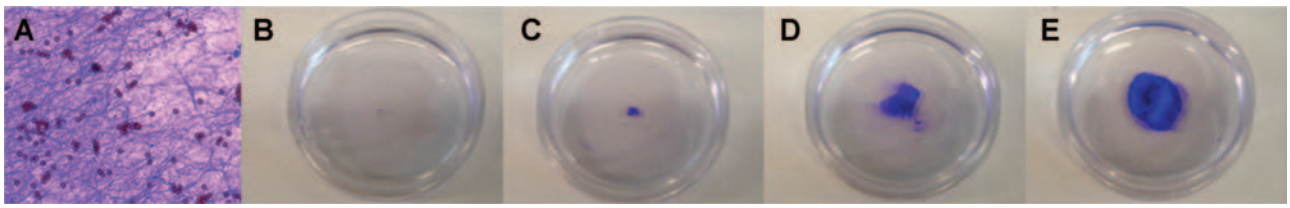

FIG. 3. Fibrin clot size depends on bead concentration. (**A**) High-magnification light micrograph of a fibrin gel induced by addition of thrombin-coated micro-beads to a fibrinogen solution after staining with Coomassie Brilliant Blue. Note the extensive numbers of blue-stained fibrin fibrils surrounding the randomly oriented beads and the lack of fibril orientation (bead diameter 4.5 μm). At the right, photographs are shown of 35-mm plastic dishes containing fibrin gels formed by 7.8×10^4 (**B**), 1.9×10^5 (**C**), 6.7×10^5 (**D**), and 4.0×10^6 (**E**) thrombin-coated beads per mL of fibrinogen solution. Clot size increased as bead concentration was raised. Color images available online at www.liebertpub.com/ten.

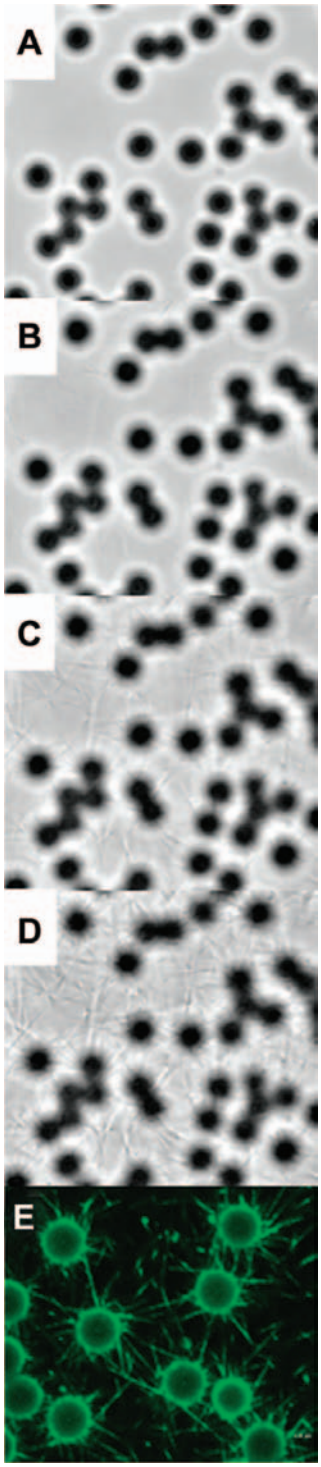

FIG. 4. Fibrin fibrils nucleate at the surface of the thrombin-coated beads. Time-lapse phase contrast images taken at 0 (**A**), 10 (**B**), 20 (**C**), and 40 (**D**) min after addition of fibrinogen solution to the beads showing progressive extension of thin fibrils from the surface of each bead until they form an intertwining fibrillar gel. (**E**) A confocal fluorescence microscopic image of a gel containing fluorescently labeled fibrinogen formed in this manner showing fibrin fibrils emanating from the surface of each bead. Color images available online at www.liebertpub.com/ten.

manner clearly shows individual fibrin fibrils extending radially from the surface of each bead (Fig. 4E).

Magnetic formation of triangulated bead arrays

Past studies on magnetically ordered crystallization of polystyrene particles immersed in ferro-fluids demonstrated that they can be magnetically oriented into triangular and chained lattices when confined to an approximately 2D region.[44,45] Other studies[46,47] have shown that groups of paramagnetic beads can be ordered in space under the influence of a magnetic field. We created a similar magnetic field configuration by suspending a stationary ring magnet and iron washer containing a small (0.125" diameter) central aperture approximately 2 cm above a fibrinogen solution containing thrombin-coated magnetic beads and thereby magnetically pulling the beads up to the air–liquid interface (Fig. 1). The geometry of the central aperture in the iron washer concentrated and redirected the magnetic fields, generating a magnetic force that pulled the beads in the sample upward and toward the center of the aperture.

When the external magnet magnetizes super-paramagnetic micro-beads present within liquid, the beads acquire a magnetization that is dependent on the external field $\vec{B}_{ext}(\vec{x})$, where $\vec{x}$ denotes the bead's spatial position. The magnet thereby pulls the magnetic beads up to the liquid–air interface and toward the center of the field with a force that depends on the angle between the bead's location and the central axis. The parallel magnetization of the beads, with bead spacing of R, also produces a bead–bead repulsion force, $\vec{F}_m(R) \propto \frac{\vec{m}^2}{R^4}$. Under these conditions, the beads should self-assemble at equilibrium into 2D regularly spaced triangular lattices (diagrammed in Fig. 1) as a result of a force balance between inter-bead repulsion due to their parallel magnetization and the concurrent force that pulls all the beads toward the center of the ring magnet.[47–49] There is an additional force due to surface tension that attracts a bead to its neighbors, but it is negligible when the beads are more than 1 bead-radius apart, as they are in this study.[47,49]

When this was carried out with magnetic micro-beads placed in PBS, a near-perfect triangular lattice of beads was produced (Fig. 5A) with an average bead–bead spacing of $19.86 \pm 0.02\,\mu m$ and a tight sample distribution (Fig. 5B). Thrombin-coated beads placed in fibrinogen solutions also formed into a fully geodesic 2D lattice at the air–liquid interface and induced fibrin clot formation without disrupting this configuration (Fig. 5C). Computerized image analysis confirmed that these samples exhibited a triangular arrangement with a tight distribution and mean bead–bead distance ($20.09 \pm 0.03\,\mu m$) (Fig. 5C, D) that was nearly identical to that produced by beads in PBS solution (Fig. 5A, B). In contrast, when fibrinogen samples containing magnetic beads were incubated in the absence of an applied magnetic field, the beads rapidly settled out into random patterns under the force of gravity (Fig. 5E); these solutions

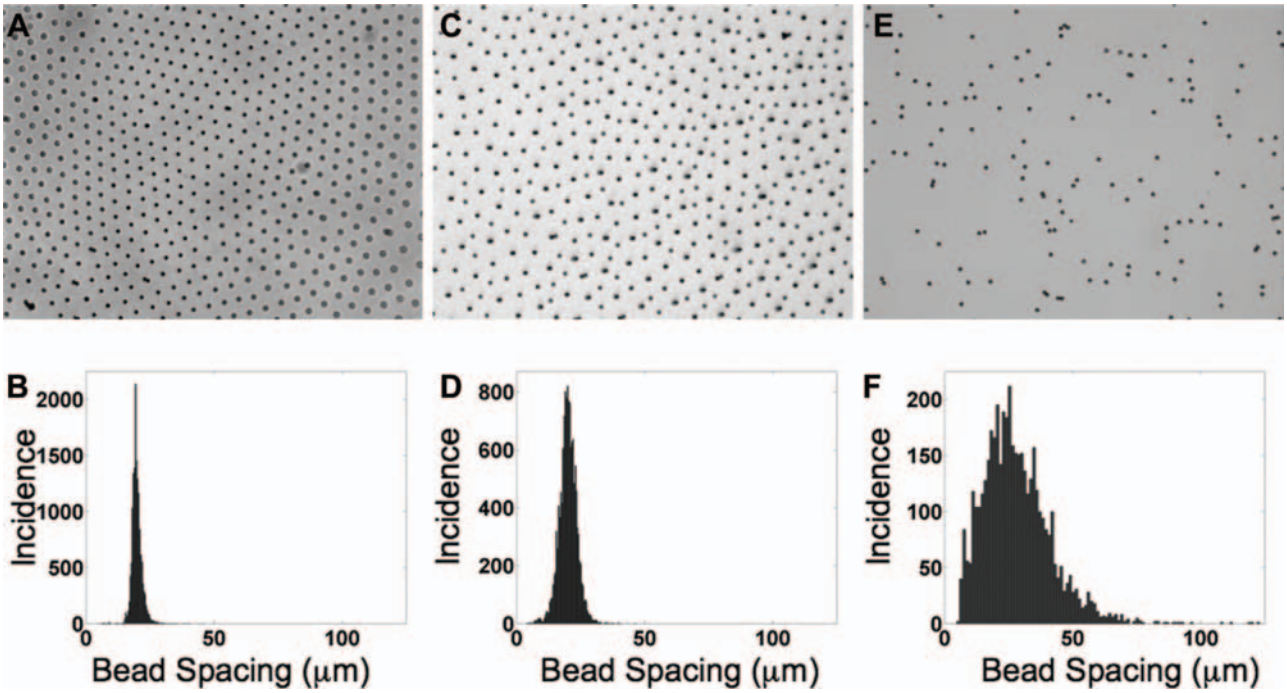

FIG. 5. Phase-contrast micrographs of bead patterns (**A, C, E**) and histograms of the inter-bead spacing distribution (**B, D, F**) within samples. Highly ordered micro-bead arrays were created with magnetic guidance when applied to beads present in phosphate-buffered saline (**A, B**) or fibrinogen solution (**C, D**) with the external magnet system, whereas random bead distributions were formed in fibrinogen solution (**E, F**) in the absence of an applied magnetic field.

had a much larger average bead–bead distance of $28.16 \pm 0.20\,\mu m$ and a broad sample distribution (Fig. 5F).

When controlled magnetic fields were used to position the beads in triangular arrays in fibrinogen solutions, the nano-meter-scale fibrin fibrils that polymerized from the beads preferentially oriented along the bead–bead axes and hence formed a similar triangulated pattern (Fig. 6A, B). To quantify the degree of fibrin fibril alignment, an orientation ratio was determined with a grid placed along the main bead–bead axis or at a 30° angle to that axis (i.e., along a line stretching from a bead to the mid point of the opposite side of the equiangular triangle formed by 3 adjacent beads; Fig. 6C). These studies revealed that the fibrin fibrils were almost 3 times (2.64 ± 0.31) as likely to be aligned along the main axis between adjacent beads than along perpendicular grid lines. In contrast, fibrils were not preferentially

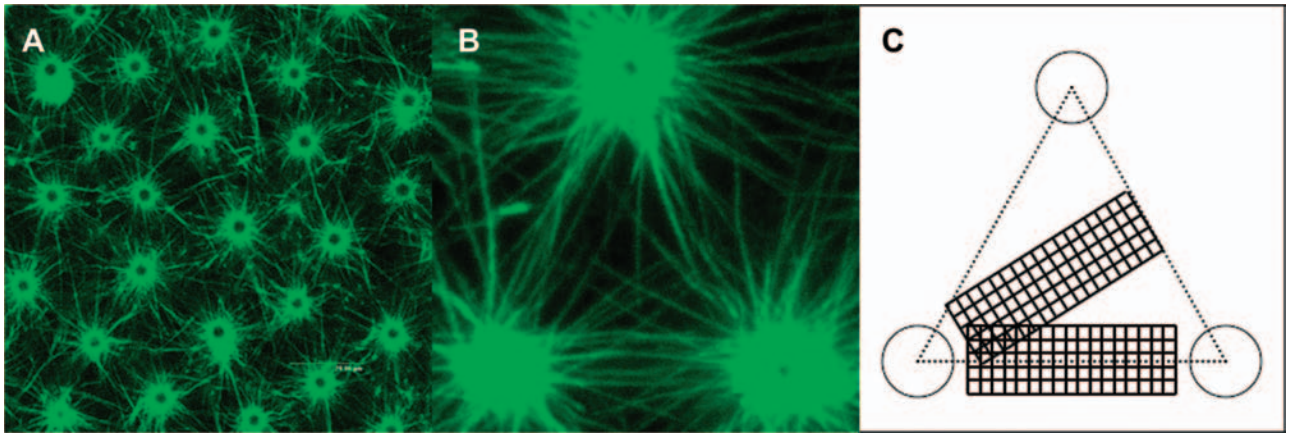

FIG. 6. Low (**A**) and high (**B**) magnification confocal microscopic images of fibrin scaffolds created with a magnetically oriented magnetic micro-bead array and a diagram showing the grid overlay system used for computerized morphometry (**C**). The high-magnification view was composed by overlaying 7 confocal Z-slices, each 1 μm apart (bead diameter 4.5 μm). Color images available online at www.liebertpub.com/ten.

oriented 30° away from the main axis between adjacent beads, because there was no enrichment of fibrils along gridlines that followed this axis relative to perpendicular gridlines (ratio = 1.13 ± 0.14).

These findings confirm that the fibrin fibrils were predominately oriented along the bead–bead axis throughout the lattice, even though fibrin monomers released by thrombin cleavage were initially in solution (i.e., only the catalytic thrombin enzyme was immobilized on the beads). Hence, fibrin lattices with defined structure on the nanometer scale can be constructed magnetically.

Cell culture on magnetically nano-structured fibrin clots

Human microvascular endothelial cells were cultured on the fibrin matrices formed by the magnetically induced arrays of thrombin-coated beads to investigate biocompatibility with the engineered substrate and to examine cell–biomaterial interactions. Cells adhered and spread well on the substrates after 4 h and remained healthy for at least 2 days in culture (Fig. 7A), thus confirming the biocompatibility of the scaffolds. As cells spread over multiple bead diameters, their peripheral attachments often inserted at sites directly above the embedded magnetic beads where the fibrin nano-fibrils were most highly concentrated (Fig. 7B). Internal actin stress fibers also aligned radially in these regions, mimicking the underlying pattern of fibrin fibrils (Fig. 7B). Direct co-alignment of actin stress fibers and underlying fibrin nano-fibrils was also observed in certain regions of the cell periphery at sites of new membrane extension (Fig. 7C), although large regions of the cells were able to extend over the substrate without apparently sensing the underlying fibrin fibril orientation (Fig. 7B, C). Nevertheless, these data show that cells can sense fibril orientation and bead location at certain times and locations and that the internal cytoskeleton reorganizes in these regions based on these local physical cues.

DISCUSSION

Cells sense and respond to nano-scale cues on the surface of planar adhesive scaffolds, such as variations in substrate topography,[50] surface roughness,[51] and adhesion ligand organization.[52] It is likely that cells within living tissues also sense and respond to 3D nano-scale features of physiological ECMs. However, developing biomaterials with defined spatial presentation of these signals on a sub-micron-length scale to control cell function has proven to be technically challenging.

In this article, we describe a novel system in which enzyme-coated magnetic micro-beads that were magnetically arranged into ordered periodic structures were used to catalyze the formation of a natural fibrin biomaterial with defined anisotropy composed of nano-meter-sized fibrillar components. Active thrombin, chemically cross-linked to the surface of magnetic micro-beads, induced fibrin clot formation as a function of bead concentration. When the beads were placed in fibrinogen solution, time-lapse and confocal microscopy confirmed that fibrin fibrils nucleated primarily from the region around the surface of the beads and extended out in a radial direction within these gels. When controlled magnetic fields were used to position the beads in hexagonal arrays, the fibrin nano-fibrils that subsequently polymerized from the beads preferentially oriented along the main bead–bead axes in a triangulated geodesic pattern. These scaffolds were biocompatible, and

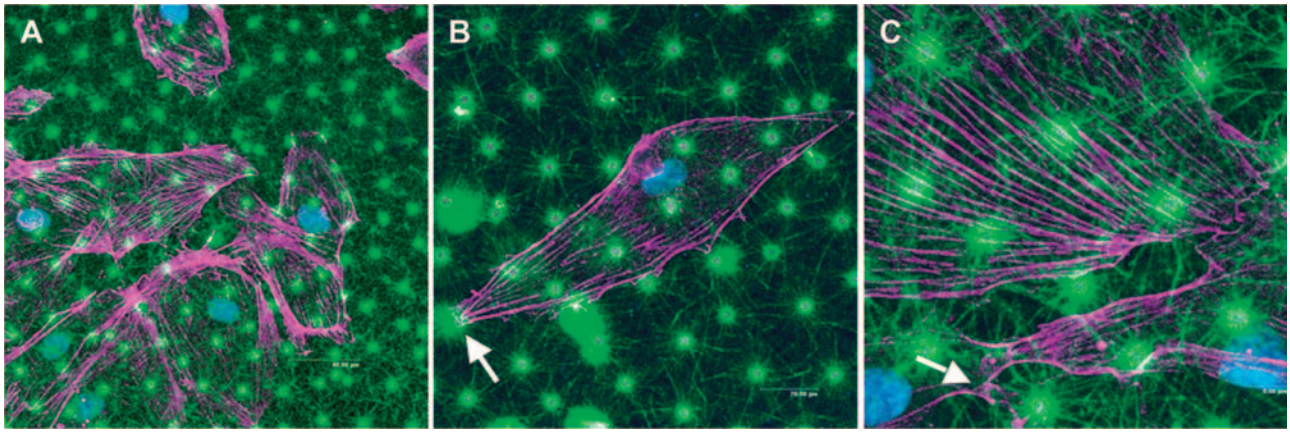

FIG. 7. Fluorescence micrographs of human microvascular endothelial cells cultured on the fibrin scaffolds (green) with defined nano-scale structure created using the magnetic fabrication technique and stained for F-actin (violet) and nuclei (blue). (**A**) Cells adhered and spread well on these scaffolds and remained viable after more than 2 days of culture. (**B**) A single cell spread over many bead diameters, which exhibits a radial array of actin stress fibers at a peripheral adhesion site near a bead (arrow) that is surrounded by a similar radial array of fibrin nano-fibrils in the clot below. (**C**) A region where multiple cells are spread over the fibrin clot; arrow indicates a small membrane extension containing 2 actin stress fibers that extend in parallel with underlying oriented fibrinogen nano-fibrils that extend radially from the surface of a nearby magnetic bead.

cultured cells could sense and respond to nano-scale structures created within the clots, as detected by co-alignment of actin stress fibers and underlying fibrin fibrils, particularly in regions of new cell extensions.

The thrombin enzyme was able to maintain its catalytic activity after being chemically coupled to the surface of the magnetic micro-beads using tosyl cross-linking chemistry. The immobilized enzyme cleaved significant quantities of thrombin-specific chromogenic substrate and formed macro-scale fibrin clots when incubated in fibrinogen solution. Even though only 2% of the thrombin provided during the coupling reaction remained bound to the beads after extensive washes, a low concentration of beads (~10^6/mL) was sufficient to create robust clots. Fibrin clot formation was clearly due to thrombin immobilized on the beads, and not soluble enzyme, because an equal volume of bead supernatant was not able to form a clot. Moreover, microscopic analysis revealed that the fibrin fibrils nucleated outward from regions near the surface of the beads. Fibril formation likely initiated in these regions because this is where the highest concentration of fibrin monomer would be present after its release from soluble fibrinogen due to the catalytic action of the immobilized thrombin enzyme.

Because clot formation is catalyzed near the surface of the beads, controlling the beads' spatial position allowed for a high degree of control over the resultant ECM structure. The nano-scale architecture of all materials governs their mechanical properties.[53] This ability to produce ECMs with customized nano-architecture may therefore facilitate future investigation of how nano-scale changes in matrix mechanics alter cell function and influence tissue repair. Spatial arrangements of the fibrin matrix are not limited to the triangular arrays reported here, because rectangular, square, and chained lattices of paramagnetic beads have also been formed at liquid—air interfaces.[46] The lattice constant, or spacing between beads, can be adjusted by changing the number of beads or the magnitudes of the peak of the field or gradient of the magnet at the sample. For a given magnet geometry, the peak field and gradient at the sample can be simply adjusted by changing the distance between the magnet and the sample; higher magnetic fields yield closer-packed lattices. The lattice shape can be altered by varying the angle between the magnetic field and the 2D plane of the air–liquid interface.[46,47,49] Low angles yield chains, and high angles yield triangular lattices. In the present study, an ideal triangulated lattice was formed when the external magnet was oriented centrally and perpendicular to the interface. Spatial manipulation of colloidal bead dispersions into numerous configurations also may be achieved by combining this magnet system with optical forces, fluid shear stresses, or electric fields;[54] template assisted self-assembly;[55] or alterations in bead volume, surface charge density, polydispersity, or electrolyte concentrations.[56]

In summary, we have developed a novel fibrin-based biomaterial with defined anisotropy composed of oriented nano-scale fibrils. These biocompatible materials were fabricated through magnetically guided assembly of a 2D array of thrombin-coated magnetic micro-beads that formed oriented fibrin fibrils through enzyme-initiated molecular self-assembly in the local micro-environment of each bead. These enzymatically active beads may be used in the future to form ordered scaffolds for a variety of applications including analysis of cell and tissue development, tissue engineering and regenerative medicine, hemorrhage control, and vascular occlusion therapy for aneurysms or cancer, as well as micro-electronics.

ACKNOWLEDGMENTS

This work was funded by Grant N00014–01–1–0782 from the Department of Defense. We thank Dr. Nicholas Geisse for helpful discussions and Gary Zabow for his technical contributions to the initial design of the external magnet apparatus.

REFERENCES

1. Giraud-Guille, M.M. Liquid crystalline order of biopolymers in cuticles and bones. Microsc Res Tech. **27,** 420, 1994.
2. Jeffery, A.K., Blunn, G.W., Archer, C.W., and Bentley, G. Three-dimensional collagen architecture in bovine articular cartilage. J Bone Joint Surg Br. **73,** 795, 1991 order.
3. Paine, M.L., and Snead, M.L. Protein interactions during assembly of the enamel organic extracellular matrix. J Bone Miner Res. **12,** 221, 1997.
4. Yurchenco, P.D., and Schittny, J.C. Molecular architecture of basement membranes. Faseb J. **4,** 1577, 1990.
5. Rakic, P. Neuronal migration and contact guidance in the primate telencephalon. Postgrad Med J. **54 Suppl 1,** 25, 1978.
6. Ingber, D.E., Madri, J.A., and Jamieson, J.D. Basement membrane as a spatial organizer of polarized epithelia. Exogenous basement membrane reorients pancreatic epithelial tumor cells *in vitro*. Am J Pathol. **122,** 129, 1986.
7. Anderson, C.R., Ponce, A.M., and Price, R.J. Immunohistochemical identification of an extracellular matrix scaffold that microguides capillary sprouting in vivo. J Histochem Cytochem. **52,** 1063, 2004.
8. Weiss, P. Nerve patterns: the mechanisms of nerve growth. Growth. **5,** 163, 1941.
9. Dubey, N., Letourneau, P.C., and Tranquillo, R.T. Neuronal contact guidance in magnetically aligned fibrin gels: effect of variation in gel mechano-structural properties. Biomaterials. **22,** 1065, 2001.
10. Lee, K.Y., and Goettler, L.A. Structure-property relationships in polymer blend nanocomposites. Polymer Eng Sci. **44,** 1103, 2004.
11. Zhang, S., Marini, D.M., Hwang, W., and Santoso, S. Design of nanostructured biological materials through self-assembly of peptides and proteins. Curr Opin Chem Biol. **6,** 865, 2002.
12. Brown, C.L., Aksay, I.A., Saville, D.A., and Hecht, M.H. Template-directed assembly of a de novo designed protein. J Am Chem Soc. **124,** 6846, 2002.

13. L'Heureux, N., Germain, L., Labbe, R., and Auger, F.A. *In vitro* construction of a human blood vessel from cultured vascular cells: a morphologic study. J Vasc Surg. **17,** 499, 1993.
14. Kanda, K., Matsuda, T., and Oka, T. *In vitro* reconstruction of hybrid vascular tissue. Hierarchic and oriented cell layers. Asaio J. **39,** M561, 1993.
15. Knight, D.P., Nash, L., Hu, X.W., Haffegee, J., and Ho, M.W. *In vitro* formation by reverse dialysis of collagen gels containing highly oriented arrays of fibrils. J Biomed Mater Res. **41,** 185, 1998.
16. Bessea, L., Coulomb, B., Lebreton-Decoster, C., and Giraud-Guille, M.M. Production of ordered collagen matrices for three-dimensional cell culture. Biomaterials. **23,** 27, 2002.
17. Torbet, J., Freyssinet, J.M., and Hudry-Clergeon, G. Oriented fibrin gels formed by polymerization in strong magnetic fields. Nature. **289,** 91, 1981.
18. Guido, S., and Tranquillo, R.T. A methodology for the systematic and quantitative study of cell contact guidance in oriented collagen gels. Correlation of fibroblast orientation and gel birefringence. J Cell Sci. **105 (Pt 2),** 317, 1993.
19. Dubey, N., Letourneau, P.C., and Tranquillo, R.T. Guided neurite elongation and schwann cell invasion into magnetically aligned collagen in simulated peripheral nerve regeneration. Exp Neurol. **158,** 338, 1999.
20. Dickinson, R.B., Guido, S., and Tranquillo, R.T. Biased cell migration of fibroblasts exhibiting contact guidance in oriented collagen gels. Ann Biomed Eng. **22,** 342, 1994.
21. Collier, J.H., Hu, B.H., Ruberti, J.W., Zhang, J., Shum, P., Thompson, D.H., and Messersmith, P.B. Thermally and photochemically triggered self-assembly of peptide hydrogels. J Am Chem Soc. **123,** 9463, 2001.
22. Holmes, T.C., de Lacalle, S., Su, X., Liu, G., Rich, A., and Zhang, S. Extensive neurite outgrowth and active synapse formation on self-assembling peptide scaffolds. Proc Natl Acad Sci U S A. **97,** 6728, 2000.
23. Yang, Z., Gu, H., Fu, D., Gao, P., Lam, J.K., and Xu, B. Enzymatic formation of supramolecular hydrogels. Adv Mater. **16,** 1440, 2004.
24. Bellomo, E.G., Wyrsta, M.D., Pakstis, L., Pochan, D.J., and Deming, T.J. Stimuli-responsive polypeptide vesicles by conformation-specific assembly. Nat Mater. **3,** 244, 2004.
25. Deming, T.J. Facile synthesis of block copolypeptides of defined architecture. Nature. **390,** 386, 1997.
26. Klok, H.A., Vandermeulen, G.W., Nuhn, H., Rosler, A., Hamley, I.W., Castelletto, V., Xu, H., and Sheiko, S.S. Peptide mediated formation of hierarchically organized solution and solid state polymer nanostructures. Faraday Discuss. **128,** 29, 2005.
27. Sidelmann, J.J., Gram, J., Jespersen, J., and Kluft, C. Fibrin clot formation and lysis: basic mechanisms. Semin Thromb Hemost. **26,** 605, 2000.
28. van Hinsbergh, V.W. The endothelium: vascular control of haemostasis. Eur J Obstet Gynecol Reprod Biol. **95,** 198, 2001.
29. Ng, A.M., Saim, A.B., Tan, K.K., Tan, G.H., Mokhtar, S.A., Rose, I.M., Othman, F., and Idrus, R.B. Comparison of bioengineered human bone construct from four sources of osteogenic cells. J Orthop Sci. **10,** 192, 2005.
30. Schmoekel, H.G., Weber, F.E., Schense, J.C., Gratz, K.W., Schawalder, P., and Hubbell, J.A. Bone repair with a form of BMP-2 engineered for incorporation into fibrin cell ingrowth matrices. Biotechnol Bioeng. **89,** 253, 2005.
31. Johnson, T.S., Xu, J.W., Zaporojan, V.V., Mesa, J.M., Weinand, C., Randolph, M.A., Bonassar, L.J., Winograd, J.M., and Yaremchuk, M.J. Integrative repair of cartilage with articular and nonarticular chondrocytes. Tissue Eng. **10,** 1308, 2004.
32. Pittier, R., Sauthier, F., Hubbell, J.A., and Hall, H. Neurite extension and *in vitro* myelination within three-dimensional modified fibrin matrices. J Neurobiol. **63,** 1, 2005.
33. Cho, S.W., Kim, S.S., Rhie, J.W., Cho, H.M., Choi, C.Y., and Kim, B.S. Engineering of volume-stable adipose tissues. Biomaterials. **26,** 3577, 2005.
34. Swartz, D.D., Russell, J.A., and Andreadis, S.T. Engineering of fibrin-based functional and implantable small-diameter blood vessels. Am J Physiol Heart Circ Physiol. **288,** H1451, 2005.
35. Ehrbar, M., Djonov, V.G., Schnell, C., Tschanz, S.A., Martiny-Baron, G., Schenk, U., Wood, J., Burri, P.H., Hubbell, J.A., and Zisch, A.H. Cell-demanded liberation of VEGF121 from fibrin implants induces local and controlled blood vessel growth. Circ Res. **94,** 1124, 2004.
36. Ryan, E.A., Mockros, L.F., Weisel, J.W., and Lorand, L. Structural origins of fibrin clot rheology. Biophys J. **77,** 2813, 1999.
37. Ferri, F., Greco, M., Arcovito, G., Bassi, F.A., De Spirito, M., Paganini, E., and Rocco, M. Growth kinetics and structure of fibrin gels. Phys Rev E Stat Nonlin Soft Matter Phys. **63,** 031401, 2001.
38. Herbert, C.B., Nagaswami, C., Bittner, G.D., Hubbell, J.A., and Weisel, J.W. Effects of fibrin micromorphology on neurite growth from dorsal root ganglia cultured in three-dimensional fibrin gels. J Biomed Mater Res. **40,** 551, 1998.
39. Wilkinson, P.C., and Lackie, J.M. The influence of contact guidance on chemotaxis of human neutrophil leukocytes. Exp Cell Res. **145,** 255, 1983.
40. Nehls, V., and Herrmann, R. The configuration of fibrin clots determines capillary morphogenesis and endothelial cell migration. Microvasc Res. **51,** 347, 1996.
41. van Hinsbergh, V.W., Collen, A., and Koolwijk, P. Role of fibrin matrix in angiogenesis. Ann N Y Acad Sci. **936,** 426, 2001.
42. Hall, H., Baechi, T., and Hubbell, J.A. Molecular properties of fibrin-based matrices for promotion of angiogenesis *in vitro*. Microvasc Res. **62,** 315, 2001.
43. Krogh, T.N., Berg, T., and Hojrup, P. Protein analysis using enzymes immobilized to paramagnetic beads. Anal Biochem. **274,** 153, 1999.
44. Skjeltorp, A.T. Colloidal crystals in magnetic fluid. J Appl Phys. **55,** 2587, 1984.
45. Skjeltorp, A.T. Ordering phenomena of particles dispersed in magnetic fluids. J Appl Phys. **57,** 3285, 1985.
46. Wen, W., Zhang, L., and Sheng, P. Planar magnetic colloidal crystals. Phys Rev Lett. **85,** 5464, 2000.
47. Helseth, L.E., and Fischer, T.M. Crystallization and chain formation in liquid drops. Phys Rev E Stat Nonlin Soft Matter Phys. **68,** 051403, 2003.
48. Golosovsky, M., Saado, Y., and Davidov, D. Energy and symmetry of self-assembled two-dimensional dipole clusters in magnetic confinement. Phys Rev E Stat Nonlin Soft Matter Phys. **65,** 061405, 2002.

49. Helseth, L.E., and Fischer, T.M. Particle interactions near the contact line in liquid drops. Phys Rev E Stat Nonlin Soft Matter Phys. **68,** 042601, 2003.
50. Andersson, A.S., Brink, J., Lidberg, U., and Sutherland, D.S. Influence of systematically varied nanoscale topography on the morphology of epithelial cells. IEEE Trans Nanobioscience. **2,** 49, 2003.
51. El-Ghannam, A.R., Ducheyne, P., Risbud, M., Adams, C.S., Shapiro, I.M., Castner, D., Golledge, S., and Composto, R.J. Model surfaces engineered with nanoscale roughness and RGD tripeptides promote osteoblast activity. J Biomed Mater Res A. **68,** 615, 2004.
52. Lee, K.Y., Alsberg, E., Hsiong, S., and Mooney, D.J. Nanoscale adhesion ligand organization regulates osteoblast proliferation and differentiation. Nanoletters. **4,** 1501, 2004.
53. Sarikaya, M., Tamerler, C., Jen, A.K., Schulten, K., and Baneyx, F. Molecular biomimetics: nanotechnology through biology. Nat Mater. **2,** 577, 2003.
54. Lowen, H. Colloidal soft matter under external control. J Phys Condens Matter. **13,** R415, 2001.
55. Yin, Y., Lu, Y., Gates, B., and Xia, Y. Template-assisted self-assembly: a practical route to complex aggregates of monodispersed colloids with well-defined sizes, shapes, and structures. J Am Chem Soc. **123,** 8718, 2001.
56. Arora, A.K., and Tata, B.V.R. Interactions, structural ordering and phase transitions in colloidal dispersions. Adv Colloid Interface Sci. **78,** 49, 1998.

Address reprint requests to:
Donald E. Ingber, M.D., Ph.D.
Vascular Biology Program
Children's Hospital/Harvard Medical School
KFRL, Room 11.127
300 Longwood Avenue
Boston, MA 02115–5737
Tel: 617–919–2223
Fax: 617–730–0230

E-mail: donald.ingber@childrens.harvard.edu